

Measurement of $e^+e^- \rightarrow K^+K^-\pi^0$ cross section and observation of a resonant structure

BESIII Collaboration

ABSTRACT: Based on e^+e^- collision data collected by the BESIII detector at the BEPCII collider at center-of-mass energies from 2.000 to 3.080 GeV, a partial-wave analysis is performed for the process $e^+e^- \rightarrow K^+K^-\pi^0$. The Born cross section of the process $e^+e^- \rightarrow K^+K^-\pi^0$ and its subprocesses $e^+e^- \rightarrow \phi\pi^0$, $K^{*+}(892)K^-$ and $K_2^{*+}(1430)K^-$ are measured. The results for $e^+e^- \rightarrow K^+K^-\pi^0$ and $\phi\pi^0$ are consistent with the BaBar measurements and with improved precision. By analyzing the cross sections of the subprocesses $e^+e^- \rightarrow K^{*+}(892)K^-$ and $K_2^{*+}(1430)K^-$, a structure with mass $M_R = (2208 \pm 19 \pm 24)$ MeV/ c^2 and width $\Gamma_R = (168 \pm 24 \pm 39)$ MeV is observed with a combined statistical significance of 7.6σ . The measured resonance parameters suggest it can be identified as the $\phi(2170)$, thus the results provide valuable input to understand the internal nature of this state.

Contents

1	Introduction	1
2	BESIII Detector and Monte Carlo simulation	2
3	Event selection and background analysis	3
4	Amplitude analysis	3
4.1	Partial wave analysis method	3
4.2	Cross section measurement	7
4.3	Systematic uncertainties for the intermediate states	7
5	Fit to the lineshapes	10
6	Summary	15
7	Acknowledgments	16

1 Introduction

The vector meson state $Y(2175)$, denoted as $\phi(2170)$ by the Particle Data Group (PDG) [1], is one of the most interesting particles in the field of light hadron spectroscopy. The $\phi(2170)$ was first observed by BaBar [2] and subsequently studied at the Belle, BESII and BESIII experiments [3–13]. Possible interpretations of the $\phi(2170)$ state include a conventional 3^3S_1 or 2^3D_1 $s\bar{s}$ state [14–17], an $s\bar{s}g$ hybrid [15, 18, 19], a tetraquark state [20–23], a $\Lambda\bar{\Lambda}(^3S_1)$ bound state [24–26], or a $\phi K\bar{K}$ resonance state [27]. The branching fractions of $\phi(2170)$ to various final states are critical probes to discriminate the different interpretations of $\phi(2170)$. For instance, the process $\phi(2170) \rightarrow K_2^{*+}(1430)K^-$ has a branching fraction an order less than the branching fraction of $\phi(2170) \rightarrow K_1^+(1400)K^-$ under the hybrid hypothesis [15, 18, 19], whereas under the conventional state hypothesis the two processes have branching fractions of the same order [14–17].

Experimentally, the $\phi(2170)$ has been studied widely in e^+e^- collisions with final states as $\phi\eta$ [13, 28], $\phi\eta'$ [12], $\phi f_0(980)$ [2–7], K^+K^- [8], $K^{*+}(892)K^{*-}(892)$ [10], and other K^+K^- states. Among the above final states, none of them is found to be the dominant decay mode, and the products of the e^+e^- partial width and the branching fraction of each final state are all less than 10 eV. The BaBar collaboration has studied the $K_2^{*+}(1430)K^-$ final state [28] by performing a Dalitz plot analysis of the process $e^+e^- \rightarrow K_S^0 K^\pm \pi^\mp$ with initial state radiation (ISR) events. The corresponding production cross section has been extracted and no structure has been found around 2.0 GeV [28]. Additionally, the measured

ratio of partial decay widths $\Gamma(\phi\eta)$ [13, 28] and $\Gamma(\phi\eta')$ [12] disfavors the hybrid interpretation [18, 19]. However, the tension can be understood by the mechanism of hadronic transition of a strangeonium-like meson along with the $\eta - \eta'$ mixing [29]. Therefore, more precise measurements of $\phi(2170)$'s decay properties are desired to reveal the internal nature of $\phi(2170)$.

In this work, we present a Partial Wave Analysis (PWA) of the process $e^+e^- \rightarrow K^+K^-\pi^0$ using data collected with the BESIII detector at center-of-mass (c.m.) energies ranging from 2.000 to 3.080 GeV with a total integrated luminosity of 648 pb $^{-1}$, where the detailed values of c.m. energy and integrated luminosities of each data set are presented in Table 1.

Table 1. Integrated luminosities of experimental data.

\sqrt{s} (GeV)	\mathcal{L} (pb $^{-1}$)	\sqrt{s} (GeV)	\mathcal{L} (pb $^{-1}$)
2.000	10.1	2.396	66.8
2.050	3.4	2.644	33.6
2.100	12.2	2.646	34.0
2.125	108.5	2.900	105.0
2.150	2.8	2.950	15.9
2.175	10.6	2.981	16.1
2.200	13.7	3.000	15.9
2.232	11.8	3.020	17.3
2.309	22.1	3.080	126.2
2.386	22.6		

2 BESIII Detector and Monte Carlo simulation

The BESIII detector [30] records symmetric e^+e^- collisions provided by the BEPCII storage ring [31], which operates with a peak luminosity of 1×10^{33} cm $^{-2}$ s $^{-1}$ in the center-of-mass energy range from 2.0 to 4.946 GeV. BESIII has collected large data samples in this energy region [32]. The cylindrical core of the BESIII detector covers 93% of the full solid angle and consists of a helium-based multilayer drift chamber (MDC), a plastic scintillator time-of-flight system (TOF), and a CsI(Tl) electromagnetic calorimeter (EMC), which are all enclosed in a superconducting solenoidal magnet providing a 1.0 T (0.9 T in 2012) magnetic field. The solenoid is supported by an octagonal flux-return yoke with resistive plate counter muon identification modules interleaved with steel. The charged-particle momentum resolution at 1 GeV/ c is 0.5%, and the dE/dx resolution is 6% for electrons from Bhabha scattering. The EMC measures photon energies with a resolution of 2.5% (5%) at 1 GeV in the barrel (end cap) region. The time resolution in the TOF barrel region is 68 ps, while that in the end cap region is 110 ps.

A Monte Carlo (MC) simulation based on GEANT4 [33], including the geometric description of the BESIII detector and its response, is used to optimize the event selection

criteria, estimate backgrounds, and determine the detection efficiency. The signal MC samples are generated using the package CONEXC [34], which incorporates a higher-order ISR correction. Background samples of the processes $e^+e^- \rightarrow e^+e^-$, $\mu^+\mu^-$ and $\gamma\gamma$ are generated with the BABAYAGA [35] generator, while $e^+e^- \rightarrow$ hadrons and two photon events are generated by the LUARLW [36] and BESTWOGAM [37] generators, respectively. Signal MC events are generated by using the amplitude model with parameters fixed to the PWA results.

3 Event selection and background analysis

The signal process under study is $e^+e^- \rightarrow K^+K^-\pi^0$ with $\pi^0 \rightarrow \gamma\gamma$. Thus, candidate events with two oppositely charged kaons and at least two photons are selected. Charged tracks detected in the MDC are required to be within a polar angle (θ) range of $|\cos\theta| < 0.93$, where θ is defined with respect to the z -axis, and their distance of closest approach to the interaction point (IP) must be less than 10 cm along the z -axis and less than 1 cm in the transverse plane. Information from TOF and dE/dx measurements is combined to form particle identification (PID) likelihoods for the π , K , and p hypotheses. Each track is assigned a particle type corresponding to the hypothesis with the highest PID likelihood. Exactly two oppositely charged kaons are required in each event. Photon candidates are identified using showers in the EMC. The deposited energy of each shower is more than 25 MeV in the barrel region ($|\cos\theta| < 0.80$) and more than 50 MeV in the end cap region ($0.86 < |\cos\theta| < 0.92$). To exclude showers induced by charged tracks, the angle between the position of each shower in the EMC and the closest extrapolated charged track is required being greater than 10° . To suppress electronic noise and showers unrelated to the event, the difference between the EMC time and the event start time is required to be within (0, 700) ns.

To improve the kinematic resolution and suppress background, a four-constraint (4C) kinematic fit imposing energy-momentum conservation is carried out under the hypothesis $e^+e^- \rightarrow K^+K^-\gamma\gamma$. If there are more than two photons, the $\gamma\gamma$ combination with minimum χ_{4C}^2 is kept for further analysis. The candidate events are required to satisfy $\chi_{4C}^2 < 65$. To suppress the contamination from the $e^+e^- \rightarrow \gamma_{ISR}\phi$ process, an additional 4C kinematic fit under the hypotheses of $e^+e^- \rightarrow K^+K^-\gamma$ is performed. The events are discarded if the corresponding χ_{4C}^2 with any photon inside the event is less than the χ_{4C}^2 of the signal hypothesis. Signal photons are required to have a $M_{\gamma\gamma}$ to be within the π^0 mass region of [0.120, 0.150] GeV/ c^2 . After applying the above selection criteria, detailed studies with MC simulation indicate that the remaining background contributions are negligible.

4 Amplitude analysis

4.1 Partial wave analysis method

Using the GPUPWA framework [38], a PWA is performed on the surviving candidate events to identify the intermediate processes presented in $e^+e^- \rightarrow K^+K^-\pi^0$. The amplitude for the $e^+e^- \rightarrow K^+K^-\pi^0$ decay is constructed with quasi two-body resonances using covariant

tensor amplitudes [39]. The intermediate states are parameterized with the relativistic Breit-Wigner (BW) functions. To include the resolution effect for the narrow ϕ resonance, a Gaussian function is convolved with the BW function. The resolution effect is negligible for the other resonances, since they have a relatively larger width. The relative magnitudes and phases of the individual intermediate processes are determined by performing an unbinned maximum likelihood fit using MINUIT [42]. Throughout the paper, charge conjugated processes are also included by default.

The PWA fit procedure begins by including all possible intermediate states in the PDG that match J^{PC} conservation in the subsequent two-body decay. These intermediate states can decay into K^+K^- or $K^\pm\pi^0$ final state. After the fit, the statistical significance of each amplitude is evaluated by incorporating the change in likelihood and degree of freedom fits with and without the corresponding amplitude included in the fit. Amplitudes with statistical significance $< 5\sigma$ are dropped. This procedure is repeated until a baseline solution is obtained with only amplitudes having a statistical significance $> 5\sigma$.

The above strategy is implemented individually on the data sets collected at $\sqrt{s} = 2.125$ and 2.396 GeV, which have the largest luminosities and yields among the nineteen data sets. The baseline solution for data at $\sqrt{s} = 2.125$ GeV includes the decay processes $e^+e^- \rightarrow \phi\pi^0$, $\rho(1450)\pi^0$, $\phi(1680)\pi^0$, $\rho(1900)\pi^0$, $\rho_3(2250)\pi^0$, $K^{*+}(832)K^-$, $K^{*+}(1410)K^-$, $K_2^{*+}(1430)K^-$, $K_3^{*+}(1780)K^-$. For data at $\sqrt{s} = 2.396$ GeV, the intermediate process $e^+e^- \rightarrow \rho(1450)\pi^0$ with a significance of 2.4σ is excluded, while the intermediate process $e^+e^- \rightarrow \phi\pi^0$ is still included in the fit to search for the possible exotic state decays to $\phi\pi^0$ [43]. The statistical significances of all intermediate processes at the two energy points are summarized in Table 2. The masses and widths of the $K_2^{*+}(1430)$, $\phi(1680)$ and $\rho(1900)$ are determined by scanning the likelihood value in the fit. The measured resonance parameters are consistent with the PDG values within uncertainty, except for the width of $K_2^*(1430)$ which is within 2 standard deviations. The masses and widths of other intermediate states are fixed to the PDG values. The resonant parameters and fit fractions of the intermediate states are summarized in Table 3 and Table 4, respectively.

Table 2. Statistical significances of possible intermediate processes at $\sqrt{s} = 2.125$ and 2.396 GeV.

Process	Significance (2.125 GeV)	Significance (2.396 GeV)
$\phi\pi^0$	18.6σ	2.3σ
$\rho(1450)\pi^0$	7.8σ	2.4σ
$\phi(1680)\pi^0$	19.5σ	14.9σ
$\rho(1900)\pi^0$	7.2σ	7.4σ
$\rho_3(2250)$	5.5σ	5.0σ
$K^*(892)K$	15.9σ	15.6σ
$K^*(1410)K$	5.7σ	5.0σ
$K_2^*(1430)K$	35.4σ	25.3σ
$K_3^*(1780)K$	5.8σ	5.5σ

Table 3. Masses and widths of the intermediate states at $\sqrt{s} = 2.125$ GeV. Due to the limited data sample size, only the statistical uncertainties are provided.

States	Mass (MeV/ c^2)	Width (MeV)	PDG Mass (MeV/ c^2)	PDG Width (MeV)
$K_2^*(1430)$	1428 ± 2	107 ± 4	1427.3 ± 1.5	100.0 ± 2.1
$\phi(1680)$	1673 ± 5	172 ± 8	1680 ± 20	150 ± 50
$\rho(1900)$	1880 ± 10	69 ± 15	$1860 - 1910$	$10 - 160$
ϕ	fixed	fixed	1019.5 ± 0.02	4.2 ± 0.01
$\rho(1450)$	fixed	fixed	1465 ± 25	400 ± 60
$\rho_3(2250)$	fixed	fixed	2248_{-17-5}^{+17+59}	$185_{-26-103}^{+31+17}$
$K^*(892)$	fixed	fixed	891.7 ± 0.3	50.8 ± 0.9
$K^*(1410)$	fixed	fixed	1414 ± 15	232 ± 21
$K_3^*(1780)$	fixed	fixed	1776 ± 7	159 ± 21

Table 4. Fit fractions of possible intermediate processes at $\sqrt{s} = 2.125$ and 2.396 GeV.

Process	Fraction (%) (2.125 GeV)	Fraction (%) (2.396 GeV)
$\phi\pi^0$	1.8 ± 0.4	0.6 ± 0.3
$\rho(1450)\pi^0$	3.8 ± 0.7	–
$\phi(1680)\pi^0$	14.6 ± 2.3	15.5 ± 2.1
$\rho(1900)\pi^0$	2.1 ± 0.3	2.7 ± 1.0
$\rho_3(2250)$	0.9 ± 0.5	0.9 ± 0.6
$K^*(892)K$	2.8 ± 0.3	9.3 ± 1.1
$K^*(1410)K$	1.1 ± 0.8	4.2 ± 1.3
$K_2^*(1430)K$	73.0 ± 3.7	66.6 ± 2.8
$K_3^*(1780)K$	1.3 ± 0.5	2.7 ± 1.4

The invariant mass spectra and angular distributions in data and fit results are shown in Figs. 1 and 2, respectively. The $\chi^2/nbin$ value is displayed on each figure to demonstrate the goodness of fit, where $nbin$ is the number of bins of each figure and χ^2 is defined as:

$$\chi^2 = \sum_{i=1}^{nbin} \frac{(n_i - \nu_i)^2}{n_i}, \quad (4.1)$$

where n_i and ν_i are the number of events for the data and the fit projections in the i th bin of each figure, respectively.

The other seventeen data samples have limited statistics, so they are fitted using the resonances from the baseline solutions obtained with $\sqrt{s} = 2.125$ GeV (for $\sqrt{s} = 2.000, 2.100, 2.175, 2.200$ and 2.232 GeV, hereafter called group I) and $\sqrt{s} = 2.396$ GeV (for the

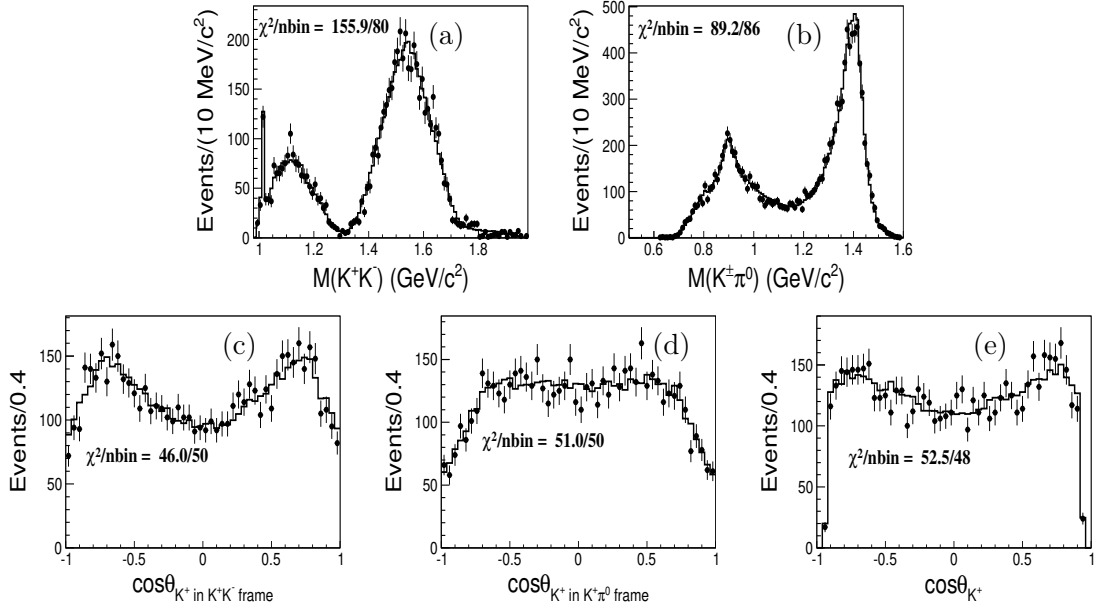


Figure 1. (a) Invariant mass distribution of K^+K^- ; (b) invariant mass distribution of $K^\pm\pi^0$; (c) $\cos\theta$ distribution of K^+ in the K^+K^- rest frame; (d) $\cos\theta$ distribution of K^+ in the $K^+\pi^0$ rest frame; (e) $\cos\theta$ distribution of K^+ in the c.m. frame at $\sqrt{s} = 2.125$ GeV. θ is polar angle with respect to the z -axis. Dots with error bars are data, and the curves are the fit results.

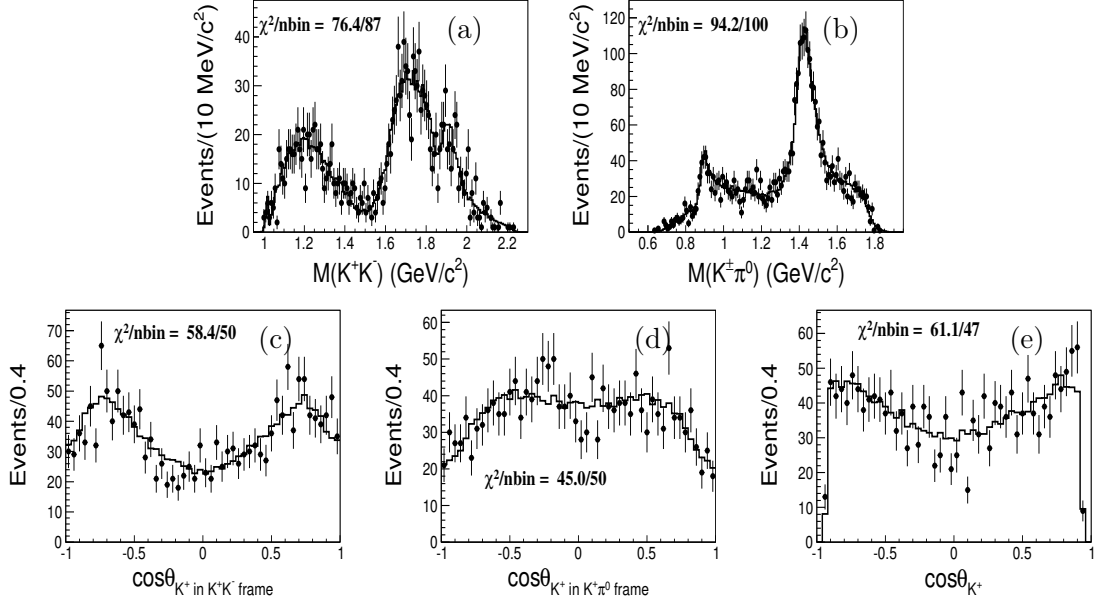


Figure 2. (a) Invariant mass distribution of K^+K^- ; (b) invariant mass distribution of $K^\pm\pi^0$; (c) $\cos\theta$ distribution of K^+ in the K^+K^- rest frame; (d) $\cos\theta$ distribution of K^+ in the $K^+\pi^0$ rest frame; (e) $\cos\theta$ distribution of K^+ in the c.m. frame at $\sqrt{s} = 2.396$ GeV. θ is polar angle with respect to the z -axis. Dots with error bars are data, and the curves are the fit results.

other data samples, hereafter named group II). For the two groups, the parameters of intermediate states are fixed, and the magnitude and phase of each process are float.

4.2 Cross section measurement

The total Born cross section for $e^+e^- \rightarrow K^+K^-\pi^0$ is obtained at the individual c.m. energy by using:

$$\sigma^{\text{B}} = \frac{N^{\text{sig}}}{\mathcal{L}_{\text{int}} \cdot \frac{1}{|1-\Pi|^2} \cdot (1+\delta)^r \cdot \mathcal{B}r \cdot \epsilon}, \quad (4.2)$$

where N^{sig} is the corresponding signal yield, which is the number of surviving events due to the negligible background; \mathcal{L}_{int} is the integrated luminosity; $(1+\delta)^r$ is the ISR correction factor obtained from QED calculations [34, 44] by incorporating the input cross section from this analysis iteratively; $\frac{1}{|1-\Pi|^2}$ is the vacuum polarization factor taken from QED calculations [45]; ϵ is the detection efficiency obtained from weighting MC simulation according to the PWA results; $\mathcal{B}r$ is the branching ratio of the decay $\pi^0 \rightarrow \gamma\gamma$ quoted from the PDG [1]. Meanwhile, the Born cross sections for the intermediate processes are obtained with the same approach, individually, while the signal yield N^{sig} is replaced with the product of the total number of surviving events and the corresponding fraction relative to the total signal yields obtained according to the PWA results, and $\mathcal{B}r$ is replaced with the product of the branching ratio of the decay $\pi^0 \rightarrow \gamma\gamma$ and that of the intermediate states quoted from the PDG [1]. The number of events of the intermediate processes, $e^+e^- \rightarrow \phi\pi^0$, $K^{*+}(892)K^-$ and $K_2^{*+}(1430)K^-$, are extracted in the PWA fit to calculate the cross section. The measured cross sections as well as the signal yields are summarized in Tables 5-8, separately for the process $e^+e^- \rightarrow K^+K^-\pi^0$ and for each individual intermediate process.

4.3 Systematic uncertainties for the intermediate states

Two categories of systematic uncertainties are considered in the measurement of the Born cross sections.

The first category includes those associated with the luminosity, track detection, PID, kinematic fit, ISR correction, and the branching fractions of intermediate states. The uncertainty associated with the integrated luminosity is 1% at each energy point [46]. The uncertainty of the detection efficiency is 1% for each charged track [47] and photon [48], individually. The PID efficiency uncertainty is 1.0% for each charged track [47]. The uncertainty related to the kinematic fit is estimated by correcting the helix parameters of the simulated charged tracks to match the resolution [49]. The uncertainty associated with the ISR and VP effect is obtained with the accuracy of the radiation function, which is about 0.5% [45], and has a contribution from the cross section lineshape, which is estimated by varying the model parameters of the fit to the cross section. All parameters are randomly varied within their uncertainties and the resulting parametrization of the lineshape is used to recalculate $(1+\delta)^r\epsilon$ and the corresponding cross section. This procedure is repeated five hundred times and the standard deviation of the resulting cross section is considered as systematic uncertainty. The uncertainty of the π^0 invariant-mass requirement is evaluated by tuning the MC sample for the π^0 mass resolution according to data at $\sqrt{s} = 2.125$

Table 5. The c.m. energy, detection efficiency, radiative correction factor, vacuum polarization factor, measured cross section for the process $e^+e^- \rightarrow K^+K^-\pi^0$, where the first uncertainties are statistical, and the second are systematic.

\sqrt{s} (GeV)	N^{sig}	ϵ (%)	$(1 + \delta)^r$	$\frac{1}{ 1-\Pi ^2}$	σ^{B} (pb)
2.000	400.0 ± 20.0	23.4	0.979	1.037	$168.4 \pm 8.4 \pm 6.6$
2.050	208.0 ± 14.4	24.5	0.962	1.038	$256.3 \pm 17.8 \pm 9.7$
2.100	712.0 ± 26.7	25.2	0.975	1.039	$232.5 \pm 8.7 \pm 9.1$
2.125	5894.0 ± 76.8	25.2	0.988	1.039	$212.2 \pm 2.8 \pm 8.1$
2.150	152.0 ± 12.3	25.4	1.000	1.040	$204.5 \pm 16.6 \pm 8.0$
2.175	504.0 ± 22.4	25.6	1.014	1.040	$178.7 \pm 8.0 \pm 7.0$
2.200	632.0 ± 25.1	24.9	1.029	1.040	$175.1 \pm 7.0 \pm 6.8$
2.232	520.0 ± 22.8	24.6	1.048	1.041	$165.5 \pm 7.3 \pm 6.3$
2.309	800.0 ± 28.3	23.7	1.091	1.041	$136.2 \pm 4.8 \pm 5.3$
2.386	636.0 ± 25.2	22.8	1.128	1.041	$106.5 \pm 4.2 \pm 4.2$
2.396	1736.0 ± 41.7	22.9	1.133	1.041	$97.4 \pm 2.3 \pm 3.8$
2.644	512.0 ± 22.6	21.5	1.205	1.039	$57.2 \pm 2.5 \pm 2.2$
2.646	560.0 ± 23.7	21.5	1.203	1.039	$62.1 \pm 2.6 \pm 2.4$
2.900	864.0 ± 29.4	21.4	1.218	1.033	$31.0 \pm 1.1 \pm 1.2$
2.950	112.0 ± 10.6	21.5	1.225	1.029	$26.3 \pm 2.5 \pm 1.1$
2.981	120.0 ± 11.0	21.1	1.230	1.025	$28.4 \pm 2.6 \pm 1.1$
3.000	124.0 ± 11.1	20.6	1.236	1.021	$30.5 \pm 2.7 \pm 1.2$
3.020	108.0 ± 10.4	21.0	1.242	1.014	$23.9 \pm 2.3 \pm 1.0$
3.080	824.0 ± 28.7	19.6	1.309	0.915	$28.2 \pm 1.0 \pm 1.1$

Table 6. The c.m. energy, detection efficiency, radiative correction factor, vacuum polarization factor, measured cross section for the process $e^+e^- \rightarrow \phi\pi^0$, where the first uncertainties are statistical, and the second are systematic.

\sqrt{s} (GeV)	N^{sig}	ϵ (%)	$(1 + \delta)^r$	$\frac{1}{ 1-\Pi ^2}$	σ^{B} (pb)
2.000	32.6 ± 10.3	17.6	1.604	1.037	$22.6 \pm 7.1 \pm 2.3$
2.050	11.3 ± 4.7	16.6	1.734	1.038	$23.3 \pm 9.7 \pm 2.3$
2.100	20.9 ± 11.8	17.5	1.671	1.039	$11.7 \pm 6.6 \pm 1.2$
2.125	106.4 ± 22.0	18.1	1.621	1.039	$6.6 \pm 1.4 \pm 0.7$
2.150	9.0 ± 3.9	18.8	1.572	1.040	$21.3 \pm 9.1 \pm 2.1$
2.175	16.9 ± 5.5	19.6	1.546	1.040	$10.4 \pm 3.4 \pm 1.0$
2.200	11.0 ± 5.3	19.3	1.592	1.040	$5.2 \pm 2.5 \pm 0.5$
2.232	6.8 ± 3.2	15.9	2.027	1.041	$3.5 \pm 1.6 \pm 0.3$
2.309	0.2 ± 0.2	9.8	3.335	1.041	$0.1 \pm 0.1 \pm 0.1$
2.386	10.5 ± 3.8	10.0	3.104	1.041	$3.0 \pm 1.1 \pm 0.3$
2.396	10.8 ± 5.5	11.0	2.860	1.041	$1.0 \pm 0.5 \pm 0.1$

Table 7. The c.m. energy, detection efficiency, radiative correction factor, vacuum polarization factor, measured cross section for the process $e^+e^- \rightarrow K_2^{*+}(1430)K^-$, where the first uncertainties are statistical, and the second are systematic.

\sqrt{s} (GeV)	N^{sig}	ϵ (%)	$(1 + \delta)^r$	$\frac{1}{ 1 - \Pi ^2}$	σ^{B} (pb)
2.000	138.5 ± 38.8	29.7	0.769	1.037	$347.6 \pm 97.5 \pm 35.3$
2.050	57.1 ± 20.2	30.5	0.797	1.038	$406.8 \pm 144.1 \pm 41.0$
2.100	413.2 ± 98.6	30.5	0.846	1.039	$764.1 \pm 182.3 \pm 77.1$
2.125	4304.1 ± 227.1	30.0	0.877	1.039	$873.3 \pm 46.1 \pm 89.0$
2.150	132.3 ± 25.5	29.4	0.902	1.040	$1015.9 \pm 196.0 \pm 103.5$
2.175	417.8 ± 53.1	29.2	0.925	1.040	$845.7 \pm 107.6 \pm 86.2$
2.200	441.4 ± 48.3	28.6	0.944	1.040	$691.7 \pm 75.6 \pm 70.5$
2.232	377.4 ± 42.6	28.3	0.963	1.041	$676.2 \pm 76.3 \pm 70.0$
2.309	548.8 ± 44.6	27.1	0.998	1.041	$531.9 \pm 43.3 \pm 29.2$
2.386	364.1 ± 30.8	26.3	1.023	1.041	$347.5 \pm 29.4 \pm 19.1$
2.396	1156.4 ± 56.1	26.2	1.025	1.041	$373.0 \pm 18.1 \pm 20.5$
2.644	339.4 ± 27.3	23.6	1.102	1.039	$225.0 \pm 18.1 \pm 12.4$
2.646	413.5 ± 27.3	23.4	1.103	1.039	$272.5 \pm 18.0 \pm 15.0$
2.900	516.7 ± 29.5	20.4	1.233	1.033	$114.0 \pm 6.5 \pm 6.3$
2.950	45.0 ± 10.0	19.6	1.268	1.029	$66.6 \pm 14.8 \pm 3.6$
2.981	52.8 ± 10.8	19.4	1.286	1.025	$77.7 \pm 15.9 \pm 4.2$
3.000	71.3 ± 11.1	19.0	1.299	1.021	$107.4 \pm 16.7 \pm 5.9$
3.020	36.4 ± 13.2	18.9	1.309	1.014	$50.6 \pm 18.4 \pm 2.8$
3.080	379.4 ± 23.7	17.6	1.352	0.915	$83.0 \pm 5.2 \pm 4.6$

GeV. The systematic uncertainties from the branching ratios of intermediate states in the subsequent decays are taken from the PDG [1] and propagated.

The second category of uncertainties are associated with the PWA fit. Fits with alternative scenarios are performed, and the changes of signal yields are taken as systematic uncertainties. Uncertainties associated with the BW parametrization are estimated by replacing the constant-width BW with the mass-dependent width. Uncertainties associated with the resonance parameters, which are taken from the PDG and fixed in the fit, are estimated by performing alternative fits with the added constraints that each resonance parameter follows a Gaussian distribution with a width equal to its uncertainty. One thousand fits are performed, and the resulting relative deviations of the signal yields are taken as systematic uncertainties. Uncertainties associated with the additional resonances are estimated by alternative fits including the components $K^*(1680)K$ or the $\rho(1700)\pi^0$, which resulted being the most significant, even if with a significance less than 5σ obtained from data. Uncertainties due to the barrier factor are estimated by varying the radius of the centrifugal barrier from 0.7 to 1.0 fm and considering the difference in σ^{B} as the uncertainty. Uncertainties associated with the MC mode for $e^+e^- \rightarrow K^+K^-\pi^0$ cross section are estimated by the alternative PWA mode including all the components with a significance more than 3σ .

Table 8. The c.m. energy, detection efficiency, radiative correction factor, vacuum polarization factor, measured cross section for the process $e^+e^- \rightarrow K^{*+}(892)K^-$, where the first uncertainties are statistical, and the second are systematic.

\sqrt{s} (GeV)	N^{sig}	ϵ (%)	$(1 + \delta)^r$	$\frac{1}{ 1-\Pi ^2}$	σ^B (pb)
2.000	23.1 ± 10.3	22.5	0.990	1.037	$30.0 \pm 13.4 \pm 3.3$
2.050	22.7 ± 9.3	23.6	0.972	1.038	$86.6 \pm 35.6 \pm 9.5$
2.100	22.3 ± 17.1	23.8	0.985	1.039	$22.9 \pm 17.6 \pm 2.5$
2.125	163.2 ± 19.8	23.7	0.997	1.039	$18.6 \pm 2.3 \pm 2.0$
2.150	5.0 ± 5.3	23.5	1.009	1.040	$21.5 \pm 23.0 \pm 2.4$
2.175	13.1 ± 7.0	23.6	1.024	1.040	$14.9 \pm 7.9 \pm 1.6$
2.200	56.0 ± 13.0	23.3	1.038	1.040	$49.4 \pm 11.4 \pm 5.4$
2.232	36.5 ± 10.8	23.2	1.057	1.041	$36.8 \pm 10.8 \pm 4.0$
2.309	76.0 ± 13.2	22.5	1.099	1.041	$40.6 \pm 7.1 \pm 1.7$
2.386	69.5 ± 14.2	22.1	1.134	1.041	$35.9 \pm 7.4 \pm 1.5$
2.396	161.6 ± 20.1	22.1	1.139	1.041	$28.1 \pm 3.5 \pm 1.2$
2.644	29.6 ± 9.1	21.2	1.211	1.039	$10.0 \pm 3.1 \pm 0.4$
2.646	24.5 ± 12.4	21.2	1.210	1.039	$8.2 \pm 4.2 \pm 0.3$
2.900	55.2 ± 10.5	21.2	1.221	1.033	$6.0 \pm 1.1 \pm 0.2$
2.950	8.0 ± 4.4	20.9	1.227	1.029	$5.8 \pm 3.2 \pm 0.2$
2.981	2.3 ± 4.1	20.9	1.233	1.025	$1.7 \pm 2.9 \pm 0.1$
3.000	1.2 ± 0.9	20.8	1.236	1.021	$0.9 \pm 0.6 \pm 0.1$
3.020	1.8 ± 3.5	20.7	1.240	1.014	$1.2 \pm 2.4 \pm 0.1$
3.080	173.1 ± 15.6	19.6	1.271	0.915	$18.3 \pm 1.7 \pm 0.8$

In the above procedure, the uncertainties associated with the barrier factor, resonance parametrization and additional resonances are strongly affected by the statistics. Thus, those uncertainties of data with $\sqrt{s}=2.125$ GeV are assigned to the group I data, while those of data with $\sqrt{s}=2.396$ GeV are assigned to the group II data. For the process $e^+e^- \rightarrow \phi\pi^0$, due to the limited statistics at $\sqrt{s}=2.396$ GeV, the uncertainties obtained at $\sqrt{s}=2.125$ GeV are assigned to all the data sets.

Assuming all the sources of systematic uncertainties as independent, the total uncertainties are the quadratic sums of the individual values, as shown in Tables 9-12, where the sources of the uncertainties tagged with ‘*’ are assumed to be 100% correlated among c.m. energies.

5 Fit to the lineshapes

The measured total Born cross sections for $e^+e^- \rightarrow K^+K^-\pi^0$ and the Born cross sections for the intermediate process $e^+e^- \rightarrow \phi\pi^0$ are shown in Fig. 3, and they are consistent with the previous results from BaBar and SND. The cross sections for the processes $e^+e^- \rightarrow K^{*+}(892)K^-$ and $K_2^{*+}(1430)K^-$ are shown in Fig. 4, where a clear peak between 2.1 GeV and 2.2 GeV is present.

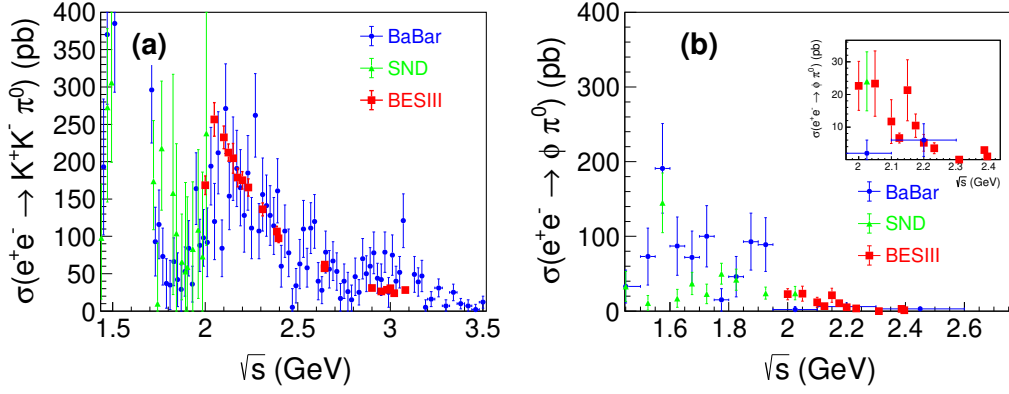


Figure 3. The Born cross sections for (a) the process $e^+e^- \rightarrow K^+K^-\pi^0$ and (b) the intermediate process $e^+e^- \rightarrow \phi\pi^0$. The red squares are from this analysis; the blue dots and the green triangles are from the BaBar [28] and SND [51] experiments, respectively.

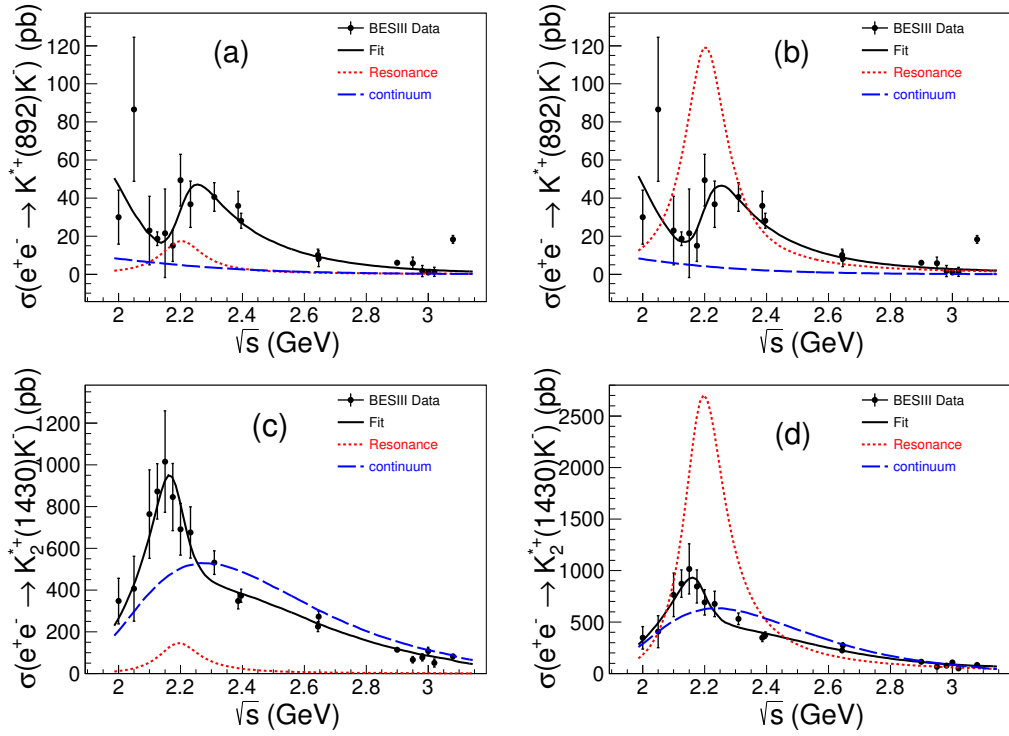


Figure 4. The Born cross section and fit curves for (a) (b) $e^+e^- \rightarrow K^{*+}(892)K^-$, and for (c) (d) $e^+e^- \rightarrow K_2^{*+}(1430)K^-$, corresponding to the two solutions in Table 13. Dots with error bars are data, where errors include both statistical and systematic uncertainties. The solid (black) curves represent for the total fit result, the short-dashed (red) curves for the intermediate state and the long-dashed (blue) curves for non-resonant component.

Table 9. Systematic uncertainties (in %) of $e^+e^- \rightarrow K^+K^-\pi^0$ at each energy point, where the sources of the uncertainties tagged with “*” are assumed to be 100% correlated among each energy point.

Data set	\mathcal{L}^*	Pho.*	Track*	PID*	π^0 Mass*	Kim.	ISR	Br*	PWA mode	Sum
2.000	1.0	2.0	2.0	2.0	0.3	0.73	1.0	0.03	0.9	3.9
2.050	1.0	2.0	2.0	2.0	0.3	0.71	0.8	0.03	0.9	3.8
2.100	1.0	2.0	2.0	2.0	0.3	0.75	1.1	0.03	0.9	3.9
2.125	1.0	2.0	2.0	2.0	0.3	0.08	0.8	0.03	0.9	3.8
2.150	1.0	2.0	2.0	2.0	0.3	0.64	1.0	0.03	0.9	3.8
2.175	1.0	2.0	2.0	2.0	0.3	0.69	0.9	0.03	0.9	3.9
2.200	1.0	2.0	2.0	2.0	0.3	0.71	0.9	0.03	0.9	3.9
2.232	1.0	2.0	2.0	2.0	0.3	0.68	0.8	0.03	0.9	3.9
2.309	1.0	2.0	2.0	2.0	0.3	0.66	0.8	0.03	1.2	3.9
2.386	1.0	2.0	2.0	2.0	0.3	0.61	0.8	0.03	1.2	3.9
2.396	1.0	2.0	2.0	2.0	0.3	0.26	0.6	0.03	1.2	3.9
2.644	1.0	2.0	2.0	2.0	0.3	0.61	0.7	0.03	1.2	3.9
2.646	1.0	2.0	2.0	2.0	0.3	0.60	0.7	0.03	1.2	3.9
2.900	1.0	2.0	2.0	2.0	0.3	0.52	1.0	0.03	1.2	4.0
2.950	1.0	2.0	2.0	2.0	0.3	0.53	1.0	0.03	1.2	4.0
2.981	1.0	2.0	2.0	2.0	0.3	0.52	1.0	0.03	1.2	4.0
3.000	1.0	2.0	2.0	2.0	0.3	0.55	1.1	0.03	1.2	4.0
3.020	1.0	2.0	2.0	2.0	0.3	0.53	1.0	0.03	1.2	4.0
3.080	1.0	2.0	2.0	2.0	0.3	0.53	1.0	0.03	1.2	4.0

To further examine the observed structure in the distributions of the measured cross sections of processes $e^+e^- \rightarrow K_2^{*+}(1430)K^-$ and $K^{*+}(892)K^-$, a χ^2 -fit, incorporating the correlated and uncorrelated uncertainties among different energy points, is performed. The fit probability density function (PDF) is a coherent sum of a non-resonant component f_1 and a resonant component f_2 :

$$\mathcal{A} = f_1 + e^{i\varphi} f_2, \quad (5.1)$$

where φ is the relative phase between the two components. The non-resonant component includes the contributions from phase space (PHSP) and low-mass resonances, and is described as [50].

$$f_1 = C_0 \cdot \sqrt{PS(\sqrt{s})} e^{-p_0(\sqrt{s}-M_{th})}, \quad (5.2)$$

Table 10. Systematic uncertainties (in %) of $e^+e^- \rightarrow \phi\pi^0$ at each energy point, where the sources of the uncertainties tagged with “*” are assumed to be 100% correlated among each energy point.

Data set	\mathcal{L}^*	Pho.*	Track*	PID*	π^0 Mass*	Kim.	ISR	Res.para	Barrer	Add.Res	Br*	Sum
2.000	1.0	2.0	2.0	2.0	0.3	1.04	0.89	1.1	5.6	9.3	1.0	11.6
2.050	1.0	2.0	2.0	2.0	0.3	1.03	0.87	1.1	5.6	9.3	1.0	11.6
2.100	1.0	2.0	2.0	2.0	0.3	0.93	0.90	1.1	5.6	9.3	1.0	11.6
2.125	1.0	2.0	2.0	2.0	0.3	0.98	0.50	1.1	5.6	9.3	1.0	11.6
2.150	1.0	2.0	2.0	2.0	0.3	0.99	0.81	1.1	5.6	9.3	1.0	11.6
2.175	1.0	2.0	2.0	2.0	0.3	0.96	0.85	1.1	5.6	9.3	1.0	11.6
2.200	1.0	2.0	2.0	2.0	0.3	0.93	0.87	1.1	5.6	9.3	1.0	11.6
2.232	1.0	2.0	2.0	2.0	0.3	0.89	0.84	1.1	5.6	9.3	1.0	11.6
2.309	1.0	2.0	2.0	2.0	0.3	0.80	0.84	1.1	5.6	9.3	1.0	11.6
2.386	1.0	2.0	2.0	2.0	0.3	0.83	0.79	1.1	5.6	9.3	1.0	11.6
2.396	1.0	2.0	2.0	2.0	0.3	0.85	0.56	1.1	5.6	9.3	1.0	11.6

Table 11. Systematic uncertainties (in %) of $e^+e^- \rightarrow K_2^{*+}(1430)K^-$ at each energy point, where the sources of the uncertainties tagged with “*” are assumed to be 100% correlated among each energy point.

Data set	\mathcal{L}^*	Pho.*	Track*	PID*	π^0 Mass*	Kim.	ISR	Res.para	Barrer	Add.Res	Br*	Sum
2.000	1.0	2.0	2.0	2.0	0.3	0.85	0.6	3.4	5.5	6.3	2.4	10.2
2.050	1.0	2.0	2.0	2.0	0.3	0.96	0.6	3.4	5.5	6.3	2.4	10.2
2.100	1.0	2.0	2.0	2.0	0.3	0.76	0.7	3.4	5.5	6.3	2.4	10.2
2.125	1.0	2.0	2.0	2.0	0.3	1.32	0.6	3.4	5.5	6.3	2.4	10.3
2.150	1.0	2.0	2.0	2.0	0.3	0.80	0.6	3.4	5.5	6.3	2.4	10.2
2.175	1.0	2.0	2.0	2.0	0.3	0.83	0.5	3.4	5.5	6.3	2.4	10.2
2.200	1.0	2.0	2.0	2.0	0.3	0.76	0.5	3.4	5.5	6.3	2.4	10.2
2.232	1.0	2.0	2.0	2.0	0.3	0.78	0.5	3.4	5.5	6.3	2.4	10.3
2.309	1.0	2.0	2.0	2.0	0.3	0.73	0.5	1.5	1.0	1.2	2.4	5.4
2.386	1.0	2.0	2.0	2.0	0.3	0.75	0.5	1.5	1.0	1.2	2.4	5.4
2.396	1.0	2.0	2.0	2.0	0.3	0.71	0.5	1.5	1.0	1.2	2.4	5.4
2.644	1.0	2.0	2.0	2.0	0.3	0.69	0.5	1.5	1.0	1.2	2.4	5.5
2.646	1.0	2.0	2.0	2.0	0.3	0.63	0.5	1.5	1.0	1.2	2.4	5.4
2.900	1.0	2.0	2.0	2.0	0.3	0.58	0.5	1.5	1.0	1.2	2.4	5.5
2.950	1.0	2.0	2.0	2.0	0.3	0.63	0.5	1.5	1.0	1.2	2.4	5.5
2.981	1.0	2.0	2.0	2.0	0.3	0.56	0.5	1.5	1.0	1.2	2.4	5.6
3.000	1.0	2.0	2.0	2.0	0.3	0.58	0.5	1.5	1.0	1.2	2.4	5.7
3.020	1.0	2.0	2.0	2.0	0.3	0.56	0.5	1.5	1.0	1.2	2.4	5.7
3.080	1.0	2.0	2.0	2.0	0.3	0.60	0.6	1.5	1.0	1.2	2.4	5.7

Table 12. Systematic uncertainties (in %) of $e^+e^- \rightarrow K^{*+}(892)K^-$ at each energy point, where the sources of the uncertainties tagged with “*” are assumed to be 100% correlated among each energy point.

Data set	L*	Pho.*	Track*	PID*	π^0 Mass*	Kim.	ISR	Res.para	Barrer	Add.Res	Br*	Sum
2.000	1.0	2.0	2.0	2.0	0.3	0.93	1.0	0.8	4.4	9.3	0.3	11.0
2.050	1.0	2.0	2.0	2.0	0.3	0.79	0.8	0.8	4.4	9.3	0.3	10.9
2.100	1.0	2.0	2.0	2.0	0.3	0.81	1.1	0.8	4.4	9.3	0.3	11.0
2.125	1.0	2.0	2.0	2.0	0.3	0.79	0.8	0.8	4.4	9.3	0.3	10.9
2.150	1.0	2.0	2.0	2.0	0.3	0.70	1.0	0.8	4.4	9.3	0.3	11.0
2.175	1.0	2.0	2.0	2.0	0.3	0.78	0.9	0.8	4.4	9.3	0.3	11.0
2.200	1.0	2.0	2.0	2.0	0.3	0.79	0.9	0.8	4.4	9.3	0.3	11.0
2.232	1.0	2.0	2.0	2.0	0.3	0.70	0.8	0.8	4.4	9.3	0.3	10.9
2.309	1.0	2.0	2.0	2.0	0.3	0.66	0.8	0.9	1.2	0.8	0.3	4.1
2.386	1.0	2.0	2.0	2.0	0.3	0.63	0.8	0.9	1.2	0.8	0.3	4.1
2.396	1.0	2.0	2.0	2.0	0.3	0.67	0.6	0.9	1.2	0.8	0.3	4.1
2.644	1.0	2.0	2.0	2.0	0.3	0.60	0.7	0.9	1.2	0.8	0.3	4.1
2.646	1.0	2.0	2.0	2.0	0.3	0.62	0.7	0.9	1.2	0.8	0.3	4.1
2.900	1.0	2.0	2.0	2.0	0.3	0.53	1.0	0.9	1.2	0.8	0.3	4.2
2.950	1.0	2.0	2.0	2.0	0.3	0.55	1.0	0.9	1.2	0.8	0.3	4.2
2.981	1.0	2.0	2.0	2.0	0.3	0.53	1.0	0.9	1.2	0.8	0.3	4.2
3.000	1.0	2.0	2.0	2.0	0.3	0.55	1.1	0.9	1.2	0.8	0.3	4.2
3.020	1.0	2.0	2.0	2.0	0.3	0.55	1.0	0.9	1.2	0.8	0.3	4.2
3.080	1.0	2.0	2.0	2.0	0.3	0.54	1.0	0.9	1.2	0.8	0.3	4.2

where $PS(\sqrt{s})$ is the PHSP distribution, C_0 and p_0 are free parameters, M_{th} is the mass threshold, $M_{th} = m_K + m_{K_2^*(1430)}$ for $K_2^{*+}(1430)K^-$ and $M_{th} = m_K + m_{K^*(892)}$ for $K^{*+}(892)K^-$. Here, the relative orbital angular momentum in the two-body decay, $L = 2$ for the process $e^+e^- \rightarrow K_2^{*+}(1430)K^-$ and $L = 1$ for the process $e^+e^- \rightarrow K^{*+}(892)K^-$, is considered in the $PS(\sqrt{s})$ [39] as it follows:

$$PS(\sqrt{s}) = \int |A_{K^{*+}(892)K^-, K_2^{*+}(1430)K^-}|^2 d\Phi_3, \quad (5.3)$$

where A is partial wave amplitude in the covariant Rarita-Schwinger tensor formalism [39], Φ_3 is three-body phase space. The amplitudes for $K_2^{*+}(1430)K^-$ and $K^{*+}(892)K^-$ are described as:

$$A_{\mu, K_2^{*+}(1430)K^-} = -\epsilon_{\mu\nu\lambda\sigma} p_\psi^\sigma \tilde{T}_{K_2^{*+}(1430)K^-}^{(2)\nu\alpha} \cdot f_{K^+\pi^0}^{K_2^{*+}} \cdot \tilde{t}_{K^+\pi^0\alpha}^{(2)\lambda}, \quad (5.4)$$

$$A_{\mu, K^{*+}(892)K^-} = -\epsilon_{\mu\nu\lambda\sigma} p_\psi^\sigma \tilde{T}_{K^{*+}(892)K^-}^{(1)\nu} \cdot f_{K^+\pi^0}^{K^{*+}} \cdot \tilde{t}_{K^+\pi^0\alpha}^{(1)\lambda}, \quad (5.5)$$

where \tilde{T}, \tilde{t} are the covariant tensors, f is a Breit-Wigner propagator [39], $\epsilon_{\mu\nu\lambda\sigma}$ is the Levi-Civita symbol, the other operators are found in reference [39].

The resonant amplitude f_2 is described with a BW function,

$$f_2 = \frac{\sqrt{12\pi \mathcal{B}r \Gamma_R^{e^+e^-} \Gamma_R}}{s - M_R^2 + iM_R\Gamma(\sqrt{s})} \cdot \sqrt{\frac{PS(\sqrt{s})}{PS(M_R)}}, \quad (5.6)$$

$$\Gamma(\sqrt{s}) = \Gamma_R \frac{PS(\sqrt{s})}{PS(M_R)}, \quad (5.7)$$

where M_R is the mass of the resonance, Γ_R is the constant width, $\Gamma_R^{e^+e^-}$ is its partial width to e^+e^- , and $\mathcal{B}r$ is the decay branching fraction to a given final state.

A simultaneous fit, assuming the same resonant structures in the $e^+e^- \rightarrow K_2^{*+}(1430)K^-$ and $K^{*+}(892)K^-$ processes, is performed to the measured cross sections. In the fit, M_R and Γ_R are shared parameters between the two processes and floating, while the production $\mathcal{B}r\Gamma_R^{e^+e^-}$ and the relative phase angle φ are independent between two processes. The fit yields two solutions with equal fit quality and identical $M_R = (2208 \pm 19)$ MeV/ c^2 and $\Gamma_R = (168 \pm 24)$ MeV. The fit curves are shown in Fig. 4, and the results are summarized in Table 13. The overall significance of this resonance is estimated to be 7.6σ for the $e^+e^- \rightarrow K_2^{*+}(1430)K^-$ and $K^{*+}(892)K^-$ processes, by comparing the change of χ^2 ($\Delta\chi^2$), with and without the resonant structure in the fit and taking the change of degrees of freedom into account. The significances of the resonant state for the two individual processes are also estimated and summarized in Table 13.

The systematic uncertainties on the resonant parameters come from the absolute c.m. energy measurement, the measured cross section, and the fit procedure. The uncertainty of the c.m. energy from BEPCII is small and is ignored in the determination of the parameters of the structure. The statistical and systematic uncertainties of the measured cross section

Table 13. A summary of fit results.

channel		$\mathcal{B}_r \Gamma_R^{e^+e^-}$ (eV)	φ (rad)	Sig. (σ)
$K_2^{*+}(1430)K^-$	solution1	8.2 ± 2.2	2.9 ± 0.3	5.7
	solution2	142.4 ± 18.7	4.8 ± 0.1	
$K^{*+}(892)K^-$	solution1	1.1 ± 0.3	3.0 ± 0.3	4.8
	solution2	6.5 ± 0.9	1.8 ± 0.1	

are incorporated in the fit, thus no further uncertainty is necessary. The uncertainties associated with the fit procedure include those from the signal model. To assess the systematic uncertainty associated with the signal model, an alternative BW function with constant width is implemented in the fit, and the resulting differences of $16.3 \text{ MeV}/c^2$ and 37.5 MeV in mass and width, respectively, are considered as the related systematic uncertainties. The uncertainty of the parametrization of the continuum contribution is estimated by changing the term $e^{-p_0(\sqrt{s}-M_{th})}$ in Eq. (5.2) with $1/s^n$, where n is a free parameter. The differences of the obtained mass and width, which are $17.2 \text{ MeV}/c^2$ and 10.0 MeV , respectively, are assigned as the corresponding systematic uncertainties. The overall systematic uncertainties are the quadratic sum of the individual ones, $23.6 \text{ MeV}/c^2$ and 38.8 MeV for the mass and width, respectively.

6 Summary

In summary, a PWA of the process $e^+e^- \rightarrow K^+K^-\pi^0$ is performed for nineteen data samples with c.m. energies between 2.000 and 3.080 GeV and a total integrated luminosity of 648 pb^{-1} taken by the BESIII detector. The Born cross section of $e^+e^- \rightarrow K^+K^-\pi^0$, as well as those for the intermediate processes $e^+e^- \rightarrow \phi\pi^0$, $K^{*+}(892)K^-$ and $K_2^{*+}(1430)K^-$, are measured by performing a PWA on each data sample individually with two baseline solutions according to its c.m. energies. The cross section for $e^+e^- \rightarrow K^+K^-\pi^0$ and $\phi\pi^0$ is measured with improved precision and is consistent with those measured by the BaBar experiment. A structure is observed in the cross section of the intermediate processes $e^+e^- \rightarrow K^{*+}(892)K^-$ and $K_2^{*+}(1430)K^-$, and by performing a simultaneous χ^2 fit, the two solutions which were obtained confirmed a resonance with mass $M_R = (2208 \pm 19 \pm 24) \text{ MeV}/c^2$, width $\Gamma_R = (168 \pm 24 \pm 39) \text{ MeV}$, and a significance of 7.6σ , where the uncertainties are statistical and systematic, respectively. The observed resonance is directly produced in e^+e^- collisions, thus a $J^{PC} = 1^{--}$ is assigned. Comparing to the vector mesons listed in the PDG [1], the mass of the observed resonance is close to those of $\phi(2170)$, $\rho(2150)$ and $\omega(2290)$, and its width is consistent with that of $\phi(2170)$ within uncertainties, but deviates from those of $\rho(2150)$ and $\omega(2290)$ by more than 3σ .

Assuming the observed structure is $\phi(2170)$, the relative branching ratio

$$R = \frac{\mathcal{B}r(\phi(2170) \rightarrow K_2^{*+}(1430)K^-)}{\mathcal{B}r(\phi(2170) \rightarrow K^{*+}(892)K^-)}$$

is calculated to be 7.5 ± 2.9 and 21.9 ± 4.2 for solution 1 and solution 2, respectively. It is noticeable that the branching fraction of $\phi(2170) \rightarrow K_2^{*+}(1430)K^-$ is significantly larger

than that of $\phi(2170) \rightarrow K^{*+}(892)K^-$, which could provide more insight into the nature of $\phi(2170)$.

7 Acknowledgments

The BESIII collaboration thanks the staff of BEPCII and the IHEP computing center and the supercomputing center of USTC for their strong support. This work is supported in part by National Key R&D Program of China under Contracts Nos. 2020YFA0406400, 2020YFA0406300; National Natural Science Foundation of China (NSFC) under Contracts Nos. 11335008, 11625523, 11635010, 11735014, 11822506, 11835012, 11935015, 11935016, 11935018, 11961141012, 12022510, 12025502, 12035009, 12035013, 12061131003, 11705192, 11975118, 11950410506, 12061131003; the Natural Science Foundation of Hunan Province under Contract Nos. 2019JJ30019 and 2020RC3054; the Chinese Academy of Sciences (CAS) Large-Scale Scientific Facility Program; Joint Large-Scale Scientific Facility Funds of the NSFC and CAS under Contracts Nos. U1732263, U1832207, U1832103, U2032111, U2032105; CAS Key Research Program of Frontier Sciences under Contract No. QYZDJ-SSW-SLH040; 100 Talents Program of CAS; INPAC and Shanghai Key Laboratory for Particle Physics and Cosmology; ERC under Contract No. 758462; European Union Horizon 2020 research and innovation programme under Contract No. Marie Skłodowska-Curie grant agreement No 894790; German Research Foundation DFG under Contracts Nos. 443159800, Collaborative Research Center CRC 1044, FOR 2359, FOR 2359, GRK 214; Istituto Nazionale di Fisica Nucleare, Italy; Ministry of Development of Turkey under Contract No. DPT2006K-120470; National Science and Technology fund; Olle Engkvist Foundation under Contract No. 200-0605; STFC (United Kingdom); The Knut and Alice Wallenberg Foundation (Sweden) under Contract No. 2016.0157; The Royal Society, UK under Contracts Nos. DH140054, DH160214; The Swedish Research Council; U. S. Department of Energy under Contracts Nos. DE-FG02-05ER41374, DE-SC-0012069.

References

- [1] P. A. Zyla *et al.* (Particle Data Group), *Prog. Theor. Exp. Phys.* **2020**, 083C01 (2020).
- [2] B. Aubert *et al.* (BaBar Collaboration), *Phys. Rev. D* **74**, 091103(R) (2006).
- [3] B. Aubert *et al.* (BaBar Collaboration), *Phys. Rev. D* **76**, 012008 (2007).
- [4] C. P. Shen *et al.* (Belle Collaboration), *Phys. Rev. D* **80**, 031101(R) (2009).
- [5] M. Ablikim *et al.* (BES Collaboration), *Phys. Rev. Lett.* **100**, 102003 (2008).
- [6] M. Ablikim *et al.* (BESIII Collaboration), *Phys. Rev. D* **91**, 052017 (2015).
- [7] M. Ablikim *et al.* (BESIII Collaboration), *Phys. Rev. D* **99**, 012014 (2019).
- [8] M. Ablikim *et al.* (BESIII Collaboration), *Phys. Rev. D* **99**, 032001 (2019).
- [9] M. Ablikim *et al.* (BESIII Collaboration), *Phys. Rev. D* **100**, 032009 (2019).
- [10] M. Ablikim *et al.* (BESIII Collaboration), *Phys. Rev. Lett.* **124**, 112001 (2020).
- [11] M. Ablikim *et al.* (BESIII Collaboration), *Phys. Lett. B* **813**, 136059 (2021).

- [12] M. Ablikim *et al.* (BESIII Collaboration), Phys. Rev. D **102**, 012008 (2020).
- [13] M. Ablikim *et al.* (BESIII Collaboration), Phys. Rev. D **104**, 032007 (2021).
- [14] T. Barnes, *et al.*, Phys. Rev. D **68** 054014 (2003).
- [15] G. J. Ding and M. L. Yan, Phys. Lett. B **657**, 49 (2007).
- [16] X. Wang *et al.*, Phys. Rev. D **85**, 074024 (2012).
- [17] S. S. Afonin and I. V. Pusenkov, Phys. Rev. D **90**, 094020 (2014).
- [18] G. J. Ding and M. L. Yan, Phys. Lett. B **650**, 390 (2007).
- [19] P. R. Page, E. S. Swanson, and A. P. Szczepaniak, Phys. Rev. D **59**, 034016 (1999).
- [20] Z. G. Wang, Nucl. Phys. A **791**, 106 (2007).
- [21] H. X. Chen *et al.*, Phys. Rev. D **78**, 034012 (2008).
- [22] H. W. Ke and X. Q. Li, Phys. Rev. D **99**, 036014 (2019).
- [23] N. V. Drenska, R. Faccini and A. D. Polosa, Phys. Lett. B **669**, 160 (2008).
- [24] L. Zhao *et al.*, Phys. Rev. D **87**, 054034 (2013).
- [25] C. Deng *et al.*, Phys. Rev. D **88**, 074007 (2013).
- [26] Y. Dong *et al.*, Phys. Rev. D **96**, 074027 (2017).
- [27] A. Martinez Torres *et al.*, Phys. Rev. D **78**, 074031 (2008); S. Gomez-Avila, M. Napsuciale and E. Oset, Phys. Rev. D **79**, 034018 (2009).
- [28] B. Aubert *et al.* (BABAR Collaboration), Phys. Rev. D **77**, 092002 (2008).
- [29] Y. Ma *et al.*, Chin. Phys. C **45**, 013112 (2021).
- [30] M. Ablikim *et al.* (BESIII Collaboration), Nucl. Instrum. Meth. A **614**, 3 (2010).
- [31] C. H. Yu *et al.*, Proceedings of IPAC2016, Busan, Korea, 2016, doi:10.18429/JACoW-IPAC2016-TUYA01.
- [32] M. Ablikim *et al.* (BESIII Collaboration), Chin. Phys. C **44**, 04000(2020).
- [33] S. Agostinelli *et al.* (GEANT4 Collaboration), Nucl. Instrum. Meth. A **506**, 250 (2003).
- [34] R. G. Ping, Chin. Phys. C **38**, 083001 (2014).
- [35] G. Balossini *et al.*, Nucl. Phys. B **758**, 227 (2006).
- [36] B. Andersson and H. Hu, arXiv:hep-ph/9910285.
- [37] M. Ablikim, *et al.* (BESIII Collaboration), Chin. Phys. C **41**, 063001 (2017).
- [38] N. Berger, B. J. Liu, and J. K. Wang, J. Phys. Conf. Ser. 219, 042031 (2010).
- [39] B. S. Zou and D. V. Bugg, Eur. Phys. J. A **16**, 537 (2003).
- [40] M. Ablikim, *et al.* (BESII Collaboration), Phys. Lett. B **598**, 149 (2004).
- [41] M. Ablikim, *et al.* (BESII Collaboration), Phys. Lett. B **645**, 19 (2007).
- [42] F. James and M. Roos, Comput. Phys. Commun. 10, 343 (1975).
- [43] F. E. Close and H. J. Lipkin, Phys. Lett. B **196**, 245 (1987).
- [44] E. A. Kuraev and V. S. Fadin, Sov. J. Nucl. Phys. **41**, 466 (1985).
- [45] S. Actis *et al.*, Eur. Phys. J. C **66**, 585 (2010).

- [46] M. Ablikim *et al.* (BESIII Collaboration), *Chin. Phys. C* **41**, 063001 (2017).
 [47] M. Ablikim *et al.* (BESIII Collaboration), *Phys. Rev. D* **99**, 032001 (2019).
 [48] M. Ablikim *et al.* (BESIII Collaboration), *Phys. Rev. D* **81**, 052005 (2010).
 [49] M. Ablikim *et al.* (BESIII Collaboration), *Phys. Rev. D* **87**, 012002 (2013).
 [50] L. Peter, *Phys. Rev. D* **98**, 113011 (2018).
 [51] M. N. Achasov *et al.* (SND Collaboration), *Eur. Phys. J. C* **80**, 1139(2020).

BESIII collaboration

M. Ablikim¹, M. N. Achasov^{10,b}, P. Adlarson⁶⁸, S. Ahmed¹⁴, M. Albrecht⁴, R. Aliberti²⁸, A. Amoroso^{67A,67C}, M. R. An³², Q. An^{64,50}, X. H. Bai⁵⁸, Y. Bai⁴⁹, O. Bakina²⁹, R. Baldini Ferroli^{23A}, I. Balossino^{24A}, Y. Ban^{39,h}, V. Batozskaya^{1,37}, D. Becker²⁸, K. Begzsuren²⁶, N. Berger²⁸, M. Bertani^{23A}, D. Bettoni^{24A}, F. Bianchi^{67A,67C}, J. Bloms⁶¹, A. Bortone^{67A,67C}, I. Boyko²⁹, R. A. Briere⁵, H. Cai⁶⁹, X. Cai^{1,50}, A. Calcaterra^{23A}, G. F. Cao^{1,55}, N. Cao^{1,55}, S. A. Cetin^{54A}, J. F. Chang^{1,50}, W. L. Chang^{1,55}, G. Chelkov^{29,a}, C. Chen³⁶, G. Chen¹, H. S. Chen^{1,55}, M. L. Chen^{1,50}, S. J. Chen³⁵, T. Chen¹, X. R. Chen²⁵, X. T. Chen¹, Y. B. Chen^{1,50}, Z. J. Chen^{20,i}, W. S. Cheng^{67C}, G. Cibinetto^{24A}, F. Cossio^{67C}, J. J. Cui⁴², X. F. Cui³⁶, H. L. Dai^{1,50}, J. P. Dai⁷¹, X. C. Dai^{1,55}, A. Dbeyssi¹⁴, R. E. de Boer⁴, D. Dedovich²⁹, Z. Y. Deng¹, A. Denig²⁸, I. Denysenko²⁹, M. Destefanis^{67A,67C}, F. De Mori^{67A,67C}, Y. Ding³³, C. Dong³⁶, J. Dong^{1,50}, L. Y. Dong^{1,55}, M. Y. Dong^{1,50,55}, X. Dong⁶⁹, S. X. Du⁷³, P. Egorov^{29,a}, Y. L. Fan⁶⁹, J. Fang^{1,50}, S. S. Fang^{1,55}, Y. Fang¹, R. Farinelli^{24A}, L. Fava^{67B,67C}, F. Feldbauer⁴, G. Felici^{23A}, C. Q. Feng^{64,50}, J. H. Feng⁵¹, M. Fritsch⁴, C. D. Fu¹, Y. Gao^{64,50}, Y. Gao^{39,h}, I. Garzia^{24A,24B}, P. T. Ge⁶⁹, C. Geng⁵¹, E. M. Gersabeck⁵⁹, A. Gilman⁶², K. Goetzen¹¹, L. Gong³³, W. X. Gong^{1,50}, W. Gradl²⁸, M. Greco^{67A,67C}, M. H. Gu^{1,50}, C. Y. Guan^{1,55}, A. Q. Guo²⁵, A. Q. Guo²², L. B. Guo³⁴, R. P. Guo⁴¹, Y. P. Guo^{9,g}, A. Guskov^{29,a}, T. T. Han⁴², W. Y. Han³², X. Q. Hao¹⁵, F. A. Harris⁵⁷, K. K. He⁴⁷, K. L. He^{1,55}, F. H. Heinsius⁴, C. H. Heinz²⁸, Y. K. Heng^{1,50,55}, C. Herold⁵², M. Himmelreich^{11,e}, T. Holtmann⁴, G. Y. Hou^{1,55}, Y. R. Hou⁵⁵, Z. L. Hou¹, H. M. Hu^{1,55}, J. F. Hu^{48,j}, T. Hu^{1,50,55}, Y. Hu¹, G. S. Huang^{64,50}, L. Q. Huang⁶⁵, X. T. Huang⁴², Y. P. Huang¹, Z. Huang^{39,h}, T. Hussain⁶⁶, N. Hüsken^{22,28}, W. Ikegami Andersson⁶⁸, W. Imoehl²², M. Irshad^{64,50}, S. Jaeger⁴, S. Janchiv²⁶, Q. Ji¹, Q. P. Ji¹⁵, X. B. Ji^{1,55}, X. L. Ji^{1,50}, Y. Y. Ji⁴², H. B. Jiang⁴², S. S. Jiang³², X. S. Jiang^{1,50,55}, J. B. Jiao⁴², Z. Jiao¹⁸, S. Jin³⁵, Y. Jin⁵⁸, M. Q. Jing^{1,55}, T. Johansson⁶⁸, N. Kalantar-Nayestanaki⁵⁶, X. S. Kang³³, R. Kappert⁵⁶, M. Kavatsyuk⁵⁶, B. C. Ke⁷³, I. K. Keshk⁴, A. Khoukaz⁶¹, P. Kiese²⁸, R. Kiuchi¹, R. Kliemt¹¹, L. Koch³⁰, O. B. Kolcu^{54A}, B. Kopf⁴, M. Kuemmel⁴, M. Kuessner⁴, A. Kupsc^{37,68}, M. G. Kurth^{1,55}, W. Kühn³⁰, J. J. Lane⁵⁹, J. S. Lange³⁰, P. Larin¹⁴, A. Lavania²¹, L. Lavezzi^{67A,67C}, Z. H. Lei^{64,50}, H. Leithoff²⁸, M. Lellmann²⁸, T. Lenz²⁸, C. Li³⁶, C. Li⁴⁰, C. H. Li³², Cheng Li^{64,50}, D. M. Li⁷³, F. Li^{1,50}, G. Li¹, H. Li⁴⁴, H. Li^{64,50}, H. B. Li^{1,55}, H. J. Li¹⁵, H. N. Li^{48,j}, J. L. Li⁴², J. Q. Li⁴, J. S. Li⁵¹, Ke Li¹, L. J Li¹, L. K. Li¹, Lei Li³, M. H. Li³⁶, P. R. Li^{31,k,l}, S. Y. Li⁵³, T. Li⁴², W. D. Li^{1,55}, W. G. Li¹, X. H. Li^{64,50}, X. L. Li⁴², Xiaoyu Li^{1,55}, Z. Y. Li⁵¹, H. Liang²⁷, H. Liang^{64,50}, H. Liang^{1,55}, Y. F. Liang⁴⁶, Y. T. Liang²⁵, G. R. Liao¹², L. Z. Liao^{1,55}, J. Libby²¹, A. Limphirat⁵², C. X. Lin⁵¹, D. X. Lin²⁵, T. Lin¹,

B. J. Liu¹, C. X. Liu¹, D. Liu^{14,64}, F. H. Liu⁴⁵, Fang Liu¹, Feng Liu⁶, G. M. Liu^{48,j},
 H. M. Liu^{1,55}, Huanhuan Liu¹, Huihui Liu¹⁶, J. B. Liu^{64,50}, J. L. Liu⁶⁵, J. Y. Liu^{1,55}, K. Liu¹,
 K. Y. Liu³³, Ke Liu¹⁷, L. Liu^{64,50}, M. H. Liu^{9,g}, P. L. Liu¹, Q. Liu⁵⁵, S. B. Liu^{64,50}, T. Liu^{9,g},
 T. Liu^{1,55}, W. M. Liu^{64,50}, X. Liu^{31,k,l}, Y. Liu^{31,k,l}, Y. B. Liu³⁶, Z. A. Liu^{1,50,55}, Z. Q. Liu⁴²,
 X. C. Lou^{1,50,55}, F. X. Lu⁵¹, H. J. Lu¹⁸, J. D. Lu^{1,55}, J. G. Lu^{1,50}, X. L. Lu¹, Y. Lu¹,
 Y. P. Lu^{1,50}, Z. H. Lu¹, C. L. Luo³⁴, M. X. Luo⁷², T. Luo^{9,g}, X. L. Luo^{1,50}, X. R. Lyu⁵⁵,
 Y. F. Lyu³⁶, F. C. Ma³³, H. L. Ma¹, L. L. Ma⁴², M. M. Ma^{1,55}, Q. M. Ma¹, R. Q. Ma^{1,55},
 R. T. Ma⁵⁵, X. X. Ma^{1,55}, X. Y. Ma^{1,50}, Y. Ma^{39,h}, F. E. Maas¹⁴, M. Maggiora^{67A,67C},
 S. Maldaner⁴, S. Malde⁶², Q. A. Malik⁶⁶, A. Mangoni^{23B}, Y. J. Mao^{39,h}, Z. P. Mao¹,
 S. Marcello^{67A,67C}, Z. X. Meng⁵⁸, J. G. Messchendorp^{56,d}, G. Mezzadri^{24A}, H. Miao¹,
 T. J. Min³⁵, R. E. Mitchell²², X. H. Mo^{1,50,55}, N. Yu. Muchnoi^{10,b}, H. Muramatsu⁶⁰,
 S. Nakhoul^{11,e}, Y. Nefedov²⁹, F. Nerling^{11,e}, I. B. Nikolaev^{10,b}, Z. Ning^{1,50}, S. Nisar^{8,m},
 S. L. Olsen⁵⁵, Q. Ouyang^{1,50,55}, S. Pacetti^{23B,23C}, X. Pan^{9,g}, Y. Pan⁵⁹, A. Pathak¹, A. Pathak²⁷,
 P. Patteri^{23A}, M. Pelizaeus⁴, H. P. Peng^{64,50}, K. Peters^{11,e}, J. Pettersson⁶⁸, J. L. Ping³⁴,
 R. G. Ping^{1,55}, S. Plura²⁸, S. Pogodin²⁹, R. Poling⁶⁰, V. Prasad^{64,50}, H. Qi^{64,50}, H. R. Qi⁵³,
 M. Qi³⁵, T. Y. Qi^{9,g}, S. Qian^{1,50}, W. B. Qian⁵⁵, Z. Qian⁵¹, C. F. Qiao⁵⁵, J. J. Qin⁶⁵,
 L. Q. Qin¹², X. P. Qin^{9,g}, X. S. Qin⁴², Z. H. Qin^{1,50}, J. F. Qiu¹, S. Q. Qu³⁶, K. H. Rashid⁶⁶,
 K. Ravindran²¹, C. F. Redmer²⁸, K. J. Ren³², A. Rivetti^{67C}, V. Rodin⁵⁶, M. Rolo^{67C},
 G. Rong^{1,55}, Ch. Rosner¹⁴, M. Rump⁶¹, H. S. Sang⁶⁴, A. Sarantsev^{29,c}, Y. Schelhaas²⁸,
 C. Schnier⁴, K. Schoenning⁶⁸, M. Scodreggio^{24A,24B}, W. Shan¹⁹, X. Y. Shan^{64,50}, J. F. Shangguan⁴⁷,
 L. G. Shao^{1,55}, M. Shao^{64,50}, C. P. Shen^{9,g}, H. F. Shen^{1,55}, X. Y. Shen^{1,55}, B.-A. Shi⁵⁵,
 H. C. Shi^{64,50}, R. S. Shi^{1,55}, X. Shi^{1,50}, X. D. Shi^{64,50}, J. J. Song¹⁵, W. M. Song^{27,1},
 Y. X. Song^{39,h}, S. Sosio^{67A,67C}, S. Spataro^{67A,67C}, F. Stieler²⁸, K. X. Su⁶⁹, P. P. Su⁴⁷,
 Y.-J. Su⁵⁵, G. X. Sun¹, H. K. Sun¹, J. F. Sun¹⁵, L. Sun⁶⁹, S. S. Sun^{1,55}, T. Sun^{1,55},
 W. Y. Sun²⁷, X. Sun^{20,i}, Y. J. Sun^{64,50}, Y. Z. Sun¹, Z. T. Sun⁴², Y. H. Tan⁶⁹, Y. X. Tan^{64,50},
 C. J. Tang⁴⁶, G. Y. Tang¹, J. Tang⁵¹, L. Y. Tao⁶⁵, Q. T. Tao^{20,i}, J. X. Teng^{64,50}, V. Thoren⁶⁸,
 W. H. Tian⁴⁴, Y. T. Tian²⁵, I. Uman^{54B}, B. Wang¹, D. Y. Wang^{39,h}, F. Wang⁶⁵, H. J. Wang^{31,k,l},
 H. P. Wang^{1,55}, K. Wang^{1,50}, L. L. Wang¹, M. Wang⁴², M. Z. Wang^{39,h}, Meng Wang^{1,55},
 S. Wang^{9,g}, T. J. Wang³⁶, W. Wang⁵¹, W. H. Wang⁶⁹, W. P. Wang^{64,50}, X. Wang^{39,h},
 X. F. Wang^{31,k,l}, X. L. Wang^{9,g}, Y. Wang⁵¹, Y. D. Wang³⁸, Y. F. Wang^{1,50,55}, Y. Q. Wang¹,
 Y. Y. Wang^{31,k,l}, Z. Wang^{1,50}, Z. Y. Wang¹, Ziyi Wang⁵⁵, Zongyuan Wang^{1,55}, D. H. Wei¹²,
 F. Weidner⁶¹, S. P. Wen¹, D. J. White⁵⁹, U. Wiedner⁴, G. Wilkinson⁶², M. Wolke⁶⁸,
 L. Wollenberg⁴, J. F. Wu^{1,55}, L. H. Wu¹, L. J. Wu^{1,55}, X. Wu^{9,g}, X. H. Wu²⁷, Z. Wu^{1,50},
 L. Xia^{64,50}, T. Xiang^{39,h}, H. Xiao^{9,g}, S. Y. Xiao¹, Z. J. Xiao³⁴, X. H. Xie^{39,h}, Y. G. Xie^{1,50},
 Y. H. Xie⁶, T. Y. Xing^{1,55}, C. F. Xu¹, C. J. Xu⁵¹, G. F. Xu¹, Q. J. Xu¹³, W. Xu^{1,55},
 X. P. Xu⁴⁷, Y. C. Xu⁵⁵, F. Yan^{9,g}, L. Yan^{9,g}, W. B. Yan^{64,50}, W. C. Yan⁷³, H. J. Yang^{43,f},
 H. X. Yang¹, L. Yang⁴⁴, S. L. Yang⁵⁵, Y. X. Yang^{1,55}, Y. X. Yang¹², Yifan Yang^{1,55},
 Zhi Yang²⁵, M. Ye^{1,50}, M. H. Ye⁷, J. H. Yin¹, Z. Y. You⁵¹, B. X. Yu^{1,50,55}, C. X. Yu³⁶,
 G. Yu^{1,55}, J. S. Yu^{20,i}, T. Yu⁶⁵, C. Z. Yuan^{1,55}, L. Yuan², S. C. Yuan¹, Y. Yuan¹, Z. Y. Yuan⁵¹,
 C. X. Yue³², A. A. Zafar⁶⁶, X. Zeng Zeng⁶, Y. Zeng^{20,i}, A. Q. Zhang¹, B. L. Zhang¹,
 B. X. Zhang¹, G. Y. Zhang¹⁵, H. Zhang⁶⁴, H. H. Zhang²⁷, H. H. Zhang⁵¹, H. Y. Zhang^{1,50},
 J. L. Zhang⁷⁰, J. Q. Zhang³⁴, J. W. Zhang^{1,50,55}, J. Y. Zhang¹, J. Z. Zhang^{1,55}, Jianyu Zhang^{1,55},
 Jiawei Zhang^{1,55}, L. M. Zhang⁵³, L. Q. Zhang⁵¹, Lei Zhang³⁵, P. Zhang¹, Shulei Zhang^{20,i},

X. D. Zhang³⁸, X. M. Zhang¹, X. Y. Zhang⁴⁷, X. Y. Zhang⁴², Y. Zhang⁶², Y. T. Zhang⁷³, Y. H. Zhang^{1,50}, Yan Zhang^{64,50}, Yao Zhang¹, Z. H. Zhang¹, Z. Y. Zhang⁶⁹, Z. Y. Zhang³⁶, G. Zhao¹, J. Zhao³², J. Y. Zhao^{1,55}, J. Z. Zhao^{1,50}, Lei Zhao^{64,50}, Ling Zhao¹, M. G. Zhao³⁶, Q. Zhao¹, S. J. Zhao⁷³, Y. B. Zhao^{1,50}, Y. X. Zhao²⁵, Z. G. Zhao^{64,50}, A. Zhemchugov^{29,a}, B. Zheng⁶⁵, J. P. Zheng^{1,50}, Y. H. Zheng⁵⁵, B. Zhong³⁴, C. Zhong⁶⁵, L. P. Zhou^{1,55}, Q. Zhou^{1,55}, X. Zhou⁶⁹, X. K. Zhou⁵⁵, X. R. Zhou^{64,50}, X. Y. Zhou³², A. N. Zhu^{1,55}, J. Zhu³⁶, K. Zhu¹, K. J. Zhu^{1,50,55}, S. H. Zhu⁶³, T. J. Zhu⁷⁰, W. J. Zhu^{9,g}, W. J. Zhu³⁶, Y. C. Zhu^{64,50}, Z. A. Zhu^{1,55}, B. S. Zou¹, J. H. Zou¹

¹ *Institute of High Energy Physics, Beijing 100049, People's Republic of China*

² *Beihang University, Beijing 100191, People's Republic of China*

³ *Beijing Institute of Petrochemical Technology, Beijing 102617, People's Republic of China*

⁴ *Bochum Ruhr-University, D-44780 Bochum, Germany*

⁵ *Carnegie Mellon University, Pittsburgh, Pennsylvania 15213, USA*

⁶ *Central China Normal University, Wuhan 430079, People's Republic of China*

⁷ *China Center of Advanced Science and Technology, Beijing 100190, People's Republic of China*

⁸ *COMSATS University Islamabad, Lahore Campus, Defence Road, Off Raiwind Road, 54000 Lahore, Pakistan*

⁹ *Fudan University, Shanghai 200443, People's Republic of China*

¹⁰ *G.I. Budker Institute of Nuclear Physics SB RAS (BINP), Novosibirsk 630090, Russia*

¹¹ *GSI Helmholtzcentre for Heavy Ion Research GmbH, D-64291 Darmstadt, Germany*

¹² *Guangxi Normal University, Guilin 541004, People's Republic of China*

¹³ *Hangzhou Normal University, Hangzhou 310036, People's Republic of China*

¹⁴ *Helmholtz Institute Mainz, Staudinger Weg 18, D-55099 Mainz, Germany*

¹⁵ *Henan Normal University, Xinxiang 453007, People's Republic of China*

¹⁶ *Henan University of Science and Technology, Luoyang 471003, People's Republic of China*

¹⁷ *Henan University of Technology, Zhengzhou 450001, People's Republic of China*

¹⁸ *Huangshan College, Huangshan 245000, People's Republic of China*

¹⁹ *Hunan Normal University, Changsha 410081, People's Republic of China*

²⁰ *Hunan University, Changsha 410082, People's Republic of China*

²¹ *Indian Institute of Technology Madras, Chennai 600036, India*

²² *Indiana University, Bloomington, Indiana 47405, USA*

²³ *INFN Laboratori Nazionali di Frascati , (A)INFN Laboratori Nazionali di Frascati, I-00044, Frascati, Italy; (B)INFN Sezione di Perugia, I-06100, Perugia, Italy; (C)University of Perugia, I-06100, Perugia, Italy*

²⁴ *INFN Sezione di Ferrara, (A)INFN Sezione di Ferrara, I-44122, Ferrara, Italy; (B)University of Ferrara, I-44122, Ferrara, Italy*

²⁵ *Institute of Modern Physics, Lanzhou 730000, People's Republic of China*

²⁶ *Institute of Physics and Technology, Peace Ave. 54B, Ulaanbaatar 13330, Mongolia*

²⁷ *Jilin University, Changchun 130012, People's Republic of China*

²⁸ *Johannes Gutenberg University of Mainz, Johann-Joachim-Becher-Weg 45, D-55099*

Mainz, Germany

²⁹ Joint Institute for Nuclear Research, 141980 Dubna, Moscow region, Russia

³⁰ Justus-Liebig-Universität Giessen, II. Physikalisches Institut, Heinrich-Buff-Ring 16, D-35392 Giessen, Germany

³¹ Lanzhou University, Lanzhou 730000, People's Republic of China

³² Liaoning Normal University, Dalian 116029, People's Republic of China

³³ Liaoning University, Shenyang 110036, People's Republic of China

³⁴ Nanjing Normal University, Nanjing 210023, People's Republic of China

³⁵ Nanjing University, Nanjing 210093, People's Republic of China

³⁶ Nankai University, Tianjin 300071, People's Republic of China

³⁷ National Centre for Nuclear Research, Warsaw 02-093, Poland

³⁸ North China Electric Power University, Beijing 102206, People's Republic of China

³⁹ Peking University, Beijing 100871, People's Republic of China

⁴⁰ Qufu Normal University, Qufu 273165, People's Republic of China

⁴¹ Shandong Normal University, Jinan 250014, People's Republic of China

⁴² Shandong University, Jinan 250100, People's Republic of China

⁴³ Shanghai Jiao Tong University, Shanghai 200240, People's Republic of China

⁴⁴ Shanxi Normal University, Linfen 041004, People's Republic of China

⁴⁵ Shanxi University, Taiyuan 030006, People's Republic of China

⁴⁶ Sichuan University, Chengdu 610064, People's Republic of China

⁴⁷ Soochow University, Suzhou 215006, People's Republic of China

⁴⁸ South China Normal University, Guangzhou 510006, People's Republic of China

⁴⁹ Southeast University, Nanjing 211100, People's Republic of China

⁵⁰ State Key Laboratory of Particle Detection and Electronics, Beijing 100049, Hefei 230026, People's Republic of China

⁵¹ Sun Yat-Sen University, Guangzhou 510275, People's Republic of China

⁵² Suranaree University of Technology, University Avenue 111, Nakhon Ratchasima 30000, Thailand

⁵³ Tsinghua University, Beijing 100084, People's Republic of China

⁵⁴ Turkish Accelerator Center Particle Factory Group, (A)Istinye University, 34010, Istanbul, Turkey; (B)Near East University, Nicosia, North Cyprus, Mersin 10, Turkey

⁵⁵ University of Chinese Academy of Sciences, Beijing 100049, People's Republic of China

⁵⁶ University of Groningen, NL-9747 AA Groningen, The Netherlands

⁵⁷ University of Hawaii, Honolulu, Hawaii 96822, USA

⁵⁸ University of Jinan, Jinan 250022, People's Republic of China

⁵⁹ University of Manchester, Oxford Road, Manchester, M13 9PL, United Kingdom

⁶⁰ University of Minnesota, Minneapolis, Minnesota 55455, USA

⁶¹ University of Muenster, Wilhelm-Klemm-Str. 9, 48149 Muenster, Germany

⁶² University of Oxford, Keble Rd, Oxford, UK OX13RH

⁶³ University of Science and Technology Liaoning, Anshan 114051, People's Republic of China

⁶⁴ University of Science and Technology of China, Hefei 230026, People's Republic of China

⁶⁵ University of South China, Hengyang 421001, People's Republic of China

- ⁶⁶ *University of the Punjab, Lahore-54590, Pakistan*
- ⁶⁷ *University of Turin and INFN, (A)University of Turin, I-10125, Turin, Italy; (B)University of Eastern Piedmont, I-15121, Alessandria, Italy; (C)INFN, I-10125, Turin, Italy*
- ⁶⁸ *Uppsala University, Box 516, SE-75120 Uppsala, Sweden*
- ⁶⁹ *Wuhan University, Wuhan 430072, People's Republic of China*
- ⁷⁰ *Xinyang Normal University, Xinyang 464000, People's Republic of China*
- ⁷¹ *Yunnan University, Kunming 650500, People's Republic of China*
- ⁷² *Zhejiang University, Hangzhou 310027, People's Republic of China*
- ⁷³ *Zhengzhou University, Zhengzhou 450001, People's Republic of China*
- ^a *Also at the Moscow Institute of Physics and Technology, Moscow 141700, Russia*
- ^b *Also at the Novosibirsk State University, Novosibirsk, 630090, Russia*
- ^c *Also at the NRC "Kurchatov Institute", PNPI, 188300, Gatchina, Russia*
- ^d *Currently at Istanbul Arel University, 34295 Istanbul, Turkey*
- ^e *Also at Goethe University Frankfurt, 60323 Frankfurt am Main, Germany*
- ^f *Also at Key Laboratory for Particle Physics, Astrophysics and Cosmology, Ministry of Education; Shanghai Key Laboratory for Particle Physics and Cosmology; Institute of Nuclear and Particle Physics, Shanghai 200240, People's Republic of China*
- ^g *Also at Key Laboratory of Nuclear Physics and Ion-beam Application (MOE) and Institute of Modern Physics, Fudan University, Shanghai 200443, People's Republic of China*
- ^h *Also at State Key Laboratory of Nuclear Physics and Technology, Peking University, Beijing 100871, People's Republic of China*
- ⁱ *Also at School of Physics and Electronics, Hunan University, Changsha 410082, China*
- ^j *Also at Guangdong Provincial Key Laboratory of Nuclear Science, Institute of Quantum Matter, South China Normal University, Guangzhou 510006, China*
- ^k *Also at Frontiers Science Center for Rare Isotopes, Lanzhou University, Lanzhou 730000, People's Republic of China*
- ^l *Also at Lanzhou Center for Theoretical Physics, Lanzhou University, Lanzhou 730000, People's Republic of China*
- ^m *Also at the Department of Mathematical Sciences, IBA, Karachi , Pakistan*